Journal of Medicinal Chemistry

Article

Structural basis and SAR for G007-LK, a lead stage 1,2,4-triazole based specific tankyrase 1/2 inhibitor

Andrey Voronkov, Daniel D Holsworth, Jo Waaler, Steven Ray Wilson, Bie Ekblad, Harmonie Perdreau-Dahl, Huyen Dinh, Gerard Drewes, Carsten Hopf, Jens Preben Morth, and Stefan Krauss

J. Med. Chem., **Just Accepted Manuscript** • DOI: 10.1021/jm4000566 • Publication Date (Web): 11 Mar 2013

Structural basis and SAR for G007-LK, a lead stage 1,2,4-triazole based specific tankyrase 1/2 inhibitor

Andrew Voronkov[1,†], Daniel D. Holsworth[1 †], Jo Waaler[1,†,*], Steven R. Wilson[2], Bie Ekblad[1], Harmonie Perdreau-Dahl[3], Huyen Dinh[1], Gerard Drewes[4], Carsten Hopf[4], Jens P. Morth[3,5]*, Stefan Krauss[1, 3] *.

Authors Affiliations:

[1] SFI CAST Biomedical Innovation Center, Unit for Cell Signaling, Oslo University Hospital, Forskningsparken, Gaustadalleén 21, 0349, Oslo, Norway, [2] Department of Chemistry, University of Oslo, P.O. Box 1033 Blindern, N-0315 Oslo, Norway,[3] Centre for Molecular Medicine Norway, Nordic EMBL Partnership, University of Oslo and Oslo University Hospital, N-0318 Oslo, Norway, [4] Cellzome AG, Meyerhofstrasse 1, 69117 Heidelberg, Germany, [5]Institute for Experimental Medical Research, Oslo University Hospital, N-0424 Oslo, Norway, [†]These authors contributed equally.

Financial Support: J.W., A.V. and B.E. and S.K. were supported by the Research Council of Norway, CRI program and Helse Sør Øst, grant 2010031.

Corresponding Authors: Jo Waaler*, Jens Preben Morth* and Stefan Krauss* (jo.waaler@rr-research.no; j.p.morth@ncmm.uio.no; Stefan.krauss@rr-research.no)

Disclosure of Potential Conflicts of Interest: The described chemical compounds are patented and may have commercial value.

Running Title: Tankyrase inhibitor, G007-LK

Key Words: Wnt/β-catenin signaling, small-molecule, inhibitor, cancer, tankyrase (TNKS).

Abbreviations: TRF1, telomeric repeat factor 1; TNKS1/2, tankyrase 1 and tankyrase 2, TRF1-interacting ankyrin-related ADP-ribose polymerase 1 and 2; PARP, poly(ADP-ribosyl)ating polymerases; GLUT4, glucose transporter type 4; IRAP, insulin responsive aminopeptidase; AXIN, Axis Inhibition Protein; KIF3a, kinesin family member 3A; NuMA, nuclear mitotic apparatus protein; IRAP, interleukin 1 receptor antagonist; Miki, mitotic kinetics regulator; CPAP, centrosomal P4.1-associated protein; 3BP2, c-Abl Src homology 3 domain-binding protein-2; RNF146, ring finger protein 146, SAR, structure-activity relationship; ST, SuperTOP; Luc, luciferase; SuperTOPFlash plasmid, ST-Luc; GMDS, GDP-mannose-4,6-dehydratase; TRAIL, TNF-related apoptosis-inducing ligand; CD95, cluster of differentiation 95; ALDOA, aldolase A; SSSCA1, Sjögren syndrome/scleroderma autoantigen 1; GPCR, G-protein coupled receptors; CYP, Cytochrome P450; CYP3A4, Cytochrome P450 3A4; SOM, site of metabolism; SCS, site of metabolism consensus score; MRCS, metabolism rate consensus score; HLM, human liver microsomes; NCS, non-crystallographic symmetry.

ABSTRACT

Tankyrases 1 and 2 (TNKS1/2) are promising pharmacological biotargets with possible applications for the development of novel anti-cancer therapeutics. A focused structure-activity relationship study was conducted based on the tankyrase inhibitor JW74 **(1)**. Chemical analoging of **1** improved the 1,2,4-triazole based core and led to 4-{5-[(E)-2-{4-(2-chlorophenyl)-5-[5-(methylsulfonyl)pyridin-2-yl]-4H-1,2,4-triazol-3-yl}ethenyl]-1,3,4-oxadiazol-2-yl}benzonitrile (G007-LK), a potent, "rule of 5" compliant and a metabolically stable TNKS1/2 inhibitor. G007-LK (**66**) displayed high selectivity toward tankyrases 1 and 2 with biochemical IC_{50}-values of 46 nM and 25 nM, respectively and a cellular IC_{50}-value of 50 nM combined with an excellent pharmacokinetic profile in mice. The PARP domain of TNKS2 was co-crystallized with **66** and the X-ray structure was determined at a 2.8 Å resolution in the space group P3221. The structure revealed that **66** binds to unique structural features in the extended adenosine binding pocket which forms the structural basis for the compounds high target selectivity and specificity. Our study provides a significantly optimized compound for targeting TNKS1/2 in vitro and in vivo.

INTRODUCTION

Adenosine diphosphate (ADP) ribosylation is a widely used catalytic process to modify proteins whereby nicotinamide adenine dinucleotide (NAD^+) is used as a substrate to form post-translational protein modifications. ADP ribosylating proteins are subdivided into mono(ADP-ribosyl)ating (ARP) and (oligo-) poly(ADP-ribosyl)ating (PARP) proteins.[1] The telomeric repeat factor 1 (TRF1)-interacting ankyrin-related ADP-ribose polymerase 1 (tankyrase 1,TNKS1, PARP5a, ARTD5; 1327 residues) and tankyrase 2 (TNKS2, PARP5b, ARTD6; 1166 residues) (TNKS1/2) belong to the subgroup of poly(ADP-ribosyl)ating polymerases. This subgroup is classified by a sterile alpha motif (SAM) domain and stretches of repetitive ankyrin domains in the N-terminus that are involved in multimerization. TNKS1/2 have been shown to poly(ADP-ribosyl)ate a number of substrate proteins by recognizing linear peptide motifs consisting of six to eight consecutive amino acids with high degeneracy.[2-6] The unique ability of tankyrase to form multimers while poly(ADP-ribosyl)ating substrate proteins led to the suggestion that tankyrases may regulate the assembly and disassembly of large polymerized structures.[7]

Tankyrases have multiple cellular functions: i) They are involved in telomere maintenance by poly(ADP-ribosyl)ating TRF1 and releasing TRF1 from telomeres.[8, 9] ii) Tankyrases are implied in vesicle transport modulating the sub-cellular distribution of glucose transporter type 4 (GLUT4) vesicles through binding to the insulin responsive aminopeptidase Interleukin 1 receptor antagonist,(IRAP),[10] and it has been shown that tankyrase, AXIN (axis inhibition protein) and KIF3a (kinesin family member 3A) form a tertiary complex that is crucial for GLUT4 sub-cellular localization.[11] iii) A role for tankyrase in spindle pole assembly through interactions with NuMA (nuclear mitotic apparatus protein) [12] and Miki (mitotic kinetics regulator)[13] . In addition, tankyrases are implied in procentriole formation through poly(ADP-

ribosyl) ation of CPAP (centrosomal P4.1-associated protein).[14] iv) A connection of TNKS1/2 to Cherubism has been established through its interaction with the 3BP2 adaptor protein (c-Abl Src homology 3 domain-binding protein-2).[2, 15] v) Recently, an involvement of tankyrase in attenuating Wnt/β-catenin signaling has been demonstrated.[16, 17] In this process, tankyrase poly(ADP-ribosyl)ates AXIN, the rate limiting structural protein in the β-catenin destruction complex. Poly(ADP-ribosyl)ation of AXIN triggers its ubiquitination initiated by the RNF146 (ring finger protein 146) ubiquitin E3 ligase followed by degradation in the proteasome.[18, 19]

Tankyrases have received attention in chemical biology as promising targets in oncology. Several small molecules have been identified that inhibit tankyrases 1 and 2, and attenuate Wnt/β-catenin signaling in reporter cell lines and in Wnt dependent cancer cell lines.[16, 17, 20, 21] Present tankyrase inhibitors can be classified into two groups: (i) Compounds that bind to the nicotinamide pocket of the PARP domain, such as 2-(4-(trifluoromethyl)phenyl)-7,8-dihydro-5H-thiopyrano[4,3-d]pyrimidin-4-ol (XAV939)[16, 22] and N-(6-Oxo-5,6-dihydrophenanthridin-2-yl)-(N,N-dimethylamino)acetamide (PJ34)[22] as well as many generic PARP inhibitors.[23, 24] (ii) Compounds that occupy the adjacent adenosine binding pocket including JW74 (**1**)[25, 26] (Figure 2a) 4-((3aR,4S,7R,7aS)-1,3-dioxo-1,3,3a,4,7,7a-hexahydro-2H-4,7-methanoisoindol-2-yl)-N-(quinolin-8-yl)benzamide (IWR-1)[27, 28], 4-((3aR,4S,7R,7aS)-1,3-dioxo-1,3,3a,4,7,7a-hexahydro-2H-4,7-methanoisoindol-2-yl)-N-(4-methylquinolin-8-yl)benzamide (IWR-2)[23, 27] and N-(4-(((4-(4-methoxyphenyl)tetrahydro-2H-pyran-4-yl)methyl)carbamoyl)phenyl)furan-2-carboxamide (JW55).[17] For clinical relevance, however, there is a need for tankyrase inhibitors with significantly improved selectivity and pharmacokinetic properties compared to existing structures. Here we describe the development of a selective and efficacious compound **1** derivative, compound G007-LK (**66**)[29] (Figure 2a), which has been stabilized against phase I

metabolism and shows an excellent pharmacokinetic profile in mice. **66** binds specifically to an extended flexible adenosine pocket of the PARP domain of TNKS1/2. We describe the molecular basis for the specific binding of the drug and describe how this interaction is the premise for the exceptionally high target selectivity observed for **66**.

RESULTS

Affinity-capture identifies TNKS1/2 as the targets of the 1,2,4-triazole based chemotype

To determine the protein target and specificity of the previously described 1,2,4-triazole based chemotype,[26] (see structure-activity relationship (SAR) paragraph), a linkable analog of compound 139 (**22**)[25](Supplementary Figure 1c), was synthesized (compound 161 (**24**)[25]**,** Figure 1a). The activity of **24** was confirmed by a cell-based ST-Luc reporter activity assay in HEK293 cells (IC_{50} [ST-Luc] = 3.92 μM, Figure 1a). Subsequently, **24** was immobilized on Sepharose beads. The **24** probe matrix was exposed to HEK293 cell extracts that had either been pre-incubated (i) with an active Wnt/β-catenin pathway inhibitor (**66)** that competes with the immobilized probes for target protein binding, (ii) with an inactive analog (compound 198, **25**)[25] or (iii) with a vehicle control (Figure 1a). The reduction in protein capture that resulted from the inhibitor treatment was quantified by isobaric tagging of tryptic peptides and tandem mass spectrometry analysis (MS/MS) of the combined peptide pools.[30] For each identified protein, the decrease of the reporter ion signals relative to the vehicle control reflected the competitive binding of the unbound inhibitor to its target. Unbound compound **66**, but not its inactive analog **25**, competed with binding of a defined set of proteins to the **24** matrix (Figure 1b). The

identified proteins were (i) tankyrases 1 and 2 (TNKS1/2), (ii) GMDS (GDP-mannose-4,6-dehydratase), a recently identified tankyrase binding protein [31] that renders colon cancer cells resistant to TRAIL (TNF-related apoptosis-inducing ligand) receptor- and CD95 (cluster of differentiation 95)-mediated apoptosis,[32] (iii) ALDOA (aldolase A), and (iv) the poorly characterized SSSCA1 (Sjögren syndrome/scleroderma autoantigen 1).

To further test whether **66** directly interfered with the catalytic activity of TNKS1/2 we used *in vitro* biochemical assays based on an NAD^+-dependent auto-poly-(ADP ribosy)lation of TNKS1/2 or PARP1 activity. **66** decreased auto-poly-(ADP ribosy)lation of TNKS1 and TNKS2 with IC_{50}-values of 46 nM and 25 nM, respectively (Supplementary Figure 4). In contrast to a benchmark compound XAV939 (**2**),[16] **66** did not show biochemical inhibition of PARP1 at doses up to 20 μM (Supplementary Figure 4). Further proof for high target specificity was established by testing **66** against a focused panel of kinases, phosphatases and G-protein coupled receptors (GPCR). **66** showed no substantial inhibition of the 90 kinases, 16 phosphatases and 73 GPCRs in the experimental setup conditions used (Supplementary Figure 5 and 6).

An important biological impact of specific inhibition of the TNKS1/2 catalytic PARP domain is an attenuation of Wnt/β-catenin signaling. By preventing poly-(ADP ribosy)lation of the tankyrase targets TNKS1/2, RNF146 and AXIN,[16, 17] Wnt/β-catenin signaling is, in a context dependent manner, decreased.[16, 17]

Structure-activity relationships establishes 66 as a phase I metabolism stabilized 1,2,4-triazole based analogue

The primary hit **1**[26] showed a moderate inhibition of tankyrase and Wnt/β-catenin signaling (IC_{50} [TNKS2] = 0.46 μM; IC_{50} [ST-Luc] = 1.01 μM) and a low phase I metabolic

stability HLM ($t_{½}$ = 3 min) (Figure 2a). During SAR development, modifications were based on H-bonding acceptor/donor potential, hydrophilic, hydrophobic and steric interactions, synthesis feasibility, impact on cLogP (<5), MW (<550), and microsomal stability assessment. In particular, compound design was guided by cLogP-values, along with *in silico* CYP metabolism consensus scores (Supplementary Figure 4c). "Rule of 5" (RO5) parameters served as a general guide for analog design. The LogP calculations were performed by using the ALOGP2.1 program, whereby an average value of several methods was applied.[33, 34] Sites of metabolism (SOM) of the proposed compounds were evaluated by consensus scoring on the basis of five software packages: MetaPrint2D, SmartCYP, MetaDrug, MetaSite and SOME[35-39] (Supplementary Figure 4 and Experimentals Section). The efficacy of new analogs was tested in a biochemical poly(ADP ribosyl)ation assay that measures the inhibition of TNKS2, and in a Wnt/β-catenin pathway assay based on ST-Luc reporter activity in Wnt3a-induced HEK293 cells (Figure 2a and Supplementary Figure 1-3). Finally, selected compounds were exposed to human liver microsomes (HLM), a suitable assay for predicting phase I metabolism (Figure 2a and Supplementary Figure 1-3). Figure 2a depicts the progress and evolution of the structure activity findings starting from molecule **1** (IC_{50} [ST-Luc] = 1.01 μM; IC_{50} [TNKS2] = 0.46 μM), highlighting selected key compounds during the process of compound improvement and ending with the lead analog **66** (IC_{50} [ST-Luc] = 0.05 μM; IC_{50} [TNKS1] = 0.046 μM; IC_{50} [TNKS2] = 0.025 μM).

Five specific regions of JW74 were selected for potential modification (Figure 2a, upper left panel). Initial SAR studies revealed that the 1,2,4-triazole core was most likely central for the activity of this chemotype. For example, when a nitrogen atom in the 1,2,4-triazole core was

replaced with a carbon atom in compound 146 (**14**),[25] activity was lost (IC_{50} [ST-Luc] > 10 μM) (Supplementary Figure 1d).

Furthermore, testing of commercially available truncated **1** analogs indicated that in the context of the central 1,2,4-triazole, regions A-D of **1** were necessary for retaining activity (Supplementary Figure 1-3). A replacement of region E by a methyl group resulted in a substantial reduction of activity (compound 264 (**54**)[29], IC_{50} [ST-Luc] = 4.5 μM, Supplementary Figure 3a). Region E was therefore retained in the further compound development.

Region C was explored to determine the contribution of the methylene thioether linkage to stability and potency. Replacing sulfur with oxygen (an H-bond acceptor) resulted in a compound devoid of activity (compound 126 (**11**)[25], IC_{50} [ST-Luc] = >10 μM; IC_{50} [TNKS2] = >10 μM) (Figure 2a). Inserting an N-H group (H bond donor) in place of sulfur also yielded an inactive molecule (compound 134 (**12**)[25], IC_{50} [ST-Luc] = >10 μM; IC_{50} [TNKS2] = >10 μM) (Figure 2a). Furthermore, **11** and **12** were unstable when exposed to HLM (Figure 2a).

A Topliss tree analysis[40] indicated an enhanced potency when there was a substitution at the 2-position of the phenyl ring (region D). The comparative analog analysis (Supplementary Figure 1c) showed also that this 2-chlorophenyl in region D yielded the best potency improvement. Together with the 1,3,4-oxadiazole ring in region B in compound 154 (**26**),[25] the potency improved 7.2 fold over **1** in a cellular assay, and 9 fold in the TNKS2 biochemical assay (**26**, IC_{50} [ST-Luc] = 0.14 μM; IC_{50} [TNKS2] = 0.051 μM) (Figure 2a). The properties of **26** indicated that metabolism may be caused by the methylene thioether moiety and/or the pyridyl group in region E (Figure 2b and Supplementary Figure 4a).[41]

Activity of compound 199 (**28**)[25](Figure 2a) (IC_{50} [ST-Luc] = 4.53 μM; IC_{50} [TNKS2] = 1.8 μM) demonstrated that a ring fusion of regions A and B can be tolerated, although a 4.5 fold loss of activity relative to **1** was seen in a cellular assay in this particular configuration.

In compound 197 (**29**)[25] (Figure 2a), a replacement of the methylene thioether moiety with an ethylene chain was tolerated with a 3.5-fold improvement in potency relatively to **1** (cellular assay), but no stability improvement against HLM was seen (t½ = 7 min) (**29**, (IC_{50} [ST-Luc] = 0.42 μM; IC_{50} [TNKS2] = 0.29 μM). Pyridine rings with a 4-substitution (region E) can metabolize via N-oxide formation, therefore it was not surprising that stability remained an issue.

Compound 251 (**43**)[25] (Figure 2a) was designed in an effort to install a stable moiety in region E while maintaining optimal moieties in regions A, B and D. Since it was envisioned that hydrogen bond acceptors and steric substitutes in the para-position of region E were favorable for potency (Supplementary Figure 2b), a methyl sulfone moiety was installed.

Furthermore, a nitrogen atom in the 2-position of the ring was installed to lower the cLogP. Compound **43** was potent (IC_{50} [ST-Luc] = 0.05 μM; IC_{50} [TNKS2] = 0.043 μM), but unstable to HLM (t½ = 4 min) (Figure 2a). This finding indicated that the methylene thio unit (region C) of **43** was the culprit of instability in HLM. However, during the course of the work, it was shown that potent tankyrase inhibitors could be derived from the 1,2,4-triazole based (**1**) chemotype.[42]

Conformational statistical analysis using Frog2 for 3D conformations, and DIVCF for clustering, was performed on compounds **1**, **26, 29** and **66**.[43,44] This analysis indicated that a trans-like conformation provides the most biologically active conformation. In addition, calculated consensus scores (MetaPrint2D, SmartCYP, MetaDrug, MetaSite) and SOM

prioritization (Figure 2b and Supplementary Figure 4), indicated that regions C and/or E were the main sources of HLM instability for compounds studied up to this point. Installation of a *trans*-alkene (mimicking the geometry of the methylene thio group) in region C (compound 244**, 55**)[29] solved the stability issue (HLM t½ = 128min), but potency (IC_{50} [ST-Luc] = 6.3 μM; IC_{50} [TNKS2] = 12.3 μM) was an issue since non-optimized groups in region A and E were present (Figure 2a).

Although region E was shown not to be required for potency (**54**, IC_{50} [ST-Luc] = 4.5 μM) (Supplementary Figure 3a), when installing the 4-sulfoxide-2-pyridyl ring in region E and methoxy group in region A of **55,** the resultant compound 268 (**65**)[29] (Figure 2a) showed improved potency (IC_{50} [ST-Luc] = 0.07 μM; IC_{50} [TNKS2] = 0.054 μM) and a favorable cLogP (3.5) profile, but exhibited reduced stability in HLM (t½ = 37 min).

Since the 3-methoxy group in region A of **65** is susceptible to demethylation, and after taking a Craig Plot replacement scheme into account, [45, 46] a 4-cyanophenyl group was installed. The resultant compound, **66**, was a potent inhibitor of TNKS1, TNKS2 and canonical Wnt/β-catenin signaling (IC_{50} [TNKS1] = 0.046 μM; IC_{50} [TNKS2] = 0.025 μM; IC_{50} [ST-Luc] = 0.05 μM) (Figure 1c and 2a). **66** had also a favorable cLogP (3.90), a high CYP3A4 inhibition IC_{50}-value (>25 μM, Supplementary Figure 4c) and was stable in HLM (t½ = 101 min, Figure 2a). Compared to the starting compound **1**, compound **66** showed 18.7 fold increased tankyrase inhibition in a biochemical assay (TNKS2 biochemical assay), and a 20.2 fold increased inhibition of ST-Luc in a cellular Wnt assay (in HEK 293 cells) while the HLM stability increased 33.7 fold. **66** has a molecular weight of 529.96 daltons and a calculated polar surface area of 140.5.

66 exhibited an excellent pharmacokinetic profile in ICR mice (Figure 2c-d). Bioavailability (F) was on average 94.3% for per oral (p.o.) administration (male: 116%, female: 72.7%) and >100% for intraperitoneal (i.p.) administration (male: 157%, female: 152%). The clearance rate (CL) was on average 520 mL/h/Kg (male: 600 mL/h/Kg, female: 430 mL/h/Kg), the volume of distribution was on average 2.42 L/Kg (male: 2.7 L/Kg, female: 2.2 L/Kg), and *in vivo* compound half-lives (t½) were on average 3.29 hours for an i.v. administration (male: 3.12, female: 3.46), 2.61 hours for a p.o. administration (male: 2.60, female: 2.63), and 2.81 hours for an i.p. administration (male: 2.89, female: 2.73)(Figure 2c-d).

Co-crystallization of 66 and TNKS2 establishes an extended adenosine binding pocket as the molecular target of 66

The drug candidate **66** was co-crystallized with the TNKS2-PARP domain residues 946-1162 including an N-terminal hexa-histidine tag and a TEV cleavage site ($TNKS2^{946-1162}$). This is identical to the constructs that were used to characterize the binding of XAV939 (**2**).[47] Soaking attempts of **66** with $TNKS2^{946-1162}$ had been unsuccessful.[48] Only prior addition of **66** to the $TNKS2^{946-1162}$ domain would form crystals and resulted in a new crystal condition with new and higher symmetry space group (P3221) (Supplementary Table 1) when compared to previous reports.[24, 28, 42, 47] Despite the relatively low pH value (pH 4.5) in the applied crystal condition, we did not expect that the acidic environment would affect the interpretation of the **66** binding properties. $TNKS2^{946-1162}$ crystallizes with three molecules in an asymmetric unit and a solvent content of ~80%. The refinement was initially performed with non-crystallographic symmetry (NCS) restrains. However, the restrains were released in the later stages of the refinement. This significantly improved the model, which implies that minor atomic differences are present

between the three molecules. The polypeptide chain of all three molecules was traced completely in the electron density map, including a fragment of the TEV cleavage peptide. There are no significant differences between the NCS related molecules as assessed by the Rapido server.[49]

The structural basis for selective binding of **66** is rationalized as a combination of hydrophobic interactions, π-π stacking, and hydrogen bond interaction formed within the adenosine binding pocket of the TNKS2-PARP domain. The drug binding pocket of **66** is primarily stabilized by hydrophobic interactions and anchored by two hydrogen bonds. One hydrogen bond is formed between the nitrogen atom (N10 in PDB ID 4HYF) of the 1,2,4-triazole core of **66** (Figure 3b) and the backbone amide of Tyr1060. The second hydrogen bond is formed between the free electron pair of the nitrogen (N16) in the oxadiazole ring (region B, Figure 3b) and the backbone amide of Asp1045. There are three key π-π stacking interactions between **66** and TNKS2: (i) The nitrile substituted aromatic ring system in region A of **66** forms a parallel π-π stacking interaction with His1048 (boxed in the alignment, Figure 3c), an equivalent interaction was previously found for the aromatic system substituted by an ether in 3-(4-methoxyphenyl)-5-((4-(4-methoxyphenyl)-5-methyl-4H-1,2,4-triazol-3-yl)thio)-1,2,4-oxadiazole (compound 24 (c24), Figure 3a).[42] ii) The chlorinated benzene ring (region D, Figure 3a and b) fits into the hydrophobic pocket that is formed by the side chains of amino acids Ser1033, Pro1034, and Tyr1071 to Ile1075 of the G-loop. We suspect that the benzene ring (region D) is supported through T-shaped π-π stacking interactions with the aromatic moiety of Phe1035 (Figure 3a and highlighted with a black box in the alignment of Figure 3c). (iii) The side chains of Tyr1060 and Tyr1071 participate in stacking interactions with the aromatic systems of region E of **66**.

In summary, we believe that the parallel π-π stacking between region A and His1048, the T-shaped π-π stacking between region D and Phe1035, the extended aromatic group in region E and the two described hydrogen bounds are core features that rationalize the efficacy and selectivity of **66**.

DISCUSSION AND CONCLUSIONS

The drug candidate **66** shows a favorable combination of high target specificity to TNKS1/2, high potency and *in vitro* as well as *in vivo* stability, leading to a good pharmacokinetic profile in mice. Earlier iTRAQ studies using the tankyrase inhibitor **2**,[16] identified TNKS1 and TNKS2, several members of the PARP family and a number of further proteins that do not contain a PARP domain. Compared to **2**, **66** shows a greater selectivity towards TNKS proteins. Furthermore, no other PARP proteins were found displaced by **66**. Interestingly, **66** displacement also enriched GMDS and SSSCA1 proteins in the eluate. Both proteins may be residing in a complex with the TNKS1/2 targets. In this context it is notable that GMDS and SSSCA1 (but not ALDOA) had also been identified by iTRAQ experiments using **2**. In contrast, known PARP1 interacting proteins such as XRCC5/6, that were found displaced by **2**,[16] were not found using the **66**-based matrix. Recently, GMDS was identified as a TNKS1 binding partner that can inhibit TNKS1 *in vitro*.[31] It is therefore a possibility that also SSSCA1 associates with TNKS proteins.

A few key binding elements in the adenosine binding pocket of TNKS2 explains the apparent high target specificity of **66**. His1048 is specific to TNKS1/2 and not conserved in other PARP domains (Figure 3c). It likely forms a parallel π–π interaction with the aromatic moiety of **66** (Figure 3a) - an interaction that has also been discussed by Shultz and co-workers for

compound **5**.[42] In addition, the molecular groove formed by the amino acids His1031 to Phe1035 (F-loop, Figure 3c) and Tyr1071 to Ile1075 (G-loop), adjacent to the nicotinamide binding pocket, have low sequence conservation throughout PARP domains in humans (Figure 3c). The structural feature of this groove is highly variable across members of the PARP family, and is in particular a distinguishing feature between tankyrases and PARP1.[50] However, the groove structure is similar in both TNKS1 and TNKS2. The molecular groove present between the G-loop and the F-loop is occupied by Tyr1203 in the apo form of TNKS1 and possibly involved in substrate release following the ADP-ribosyltransferase reaction and NAD^+ exchange binding by Tyr1203 (TNKS2 numbering Tyr1050),[50] whereby Tyr1203forms a hydrogen bond with the backbone carbonyl of Tyr1224 (equivalent toTyr1071). Thus both **66** and **5** are predicted to interfere sterically with a natural binding site of Tyr1050 from the D-loop. It is widely accepted that antagonistic drugs ensure specificity by hitting key functional elements in the binding pocket. Examples of this have been described for the quinazolinone and pyridol-pyrimidine classes of p38 mitogen-activated protein (MAP) kinase inhibitors, a class of kinase inhibitors with a high degree of specificity due to a p38 MAP kinase flexible region (Met109-Gly110) that allows a peptide flip to accommodate the inhibitor binding.[51]

Interestingly, the conserved loop motif between beta3 and alpha3 [HQ]-[GQ]-[STV], found in all human PARPs (Figure 3c), extends into Pro1034-Phe1035 in the TNKS-PARP domain. This forms a unique structural motif that is only found in tankyrases. It may be speculated that the positioning of both **66** and **5**[42] in the binding pocket of tankyrase might be guided in combination by His1048 and Phe1035. Furthermore, we interpret the clear density of the chloride position in the anomalous difference density map as an indicator for possible significant hydrophobic interactions that guide the compound placement in the pocket.

Although there are clear similarities between the binding of IWR-1 (**3**), PJ34 (**4**)[22], c24 (**5**) and **66**, there are also significant differences. In particular the D-loop (Phe1044-Ile1059) with residue Tyr1050 seems to be forced away by **66**. This D-loop feature is not present for **5** and **3**, when comparing to the drug pocket of TNKS1 derived from co-crystallography with **5** (PDB ID 3UDD)[42] and in the drug pocket of TNKS2 derived from co-crystallography with IWR-1 (PDB ID 3UA9)[28]. We hypothesize that the benzene/sulfone moiety of **66** forces the D-loop to allow an induced fit between Tyr1060 and Tyr1071. This may also contribute significantly to the specificity of **66**.

The drug pocket itself, in the presence of **66** and **5,** is dry, no water molecules have been modelled in between **66** or **5** and TNKS2 to form intercalating hydrogen bonds. Indeed there are no water molecules that seem to directly support the binding affinity. Thus the dynamics of how NAD^+ enter the pocket in the catalytic process forming poly(APD-ribosyl) chains and the ability of **66** to interfere with the process at the molecular level should be features to study in future scientific interrogation.

The novel tankyrase inhibitor **66** extends the possibilities to selectively inhibit TNKS1/2 *in vitro* and *in vivo*. As such, **66** provides an excellent small-molecule for analyzing the functions of TNKS1/2, Wnt/β-catenin signaling in cell biology, cancer and disease models.

EXPERIMENTALS SECTION

Chemistry. The following catalog compounds were purchased: **1** (Ambinter) and **26** (ChemRoyal). The following compounds were synthesized and purchased: **10**, **11**, **28**, **29,** (Medicilon) and **43**, **55**, **65** and **66** (TC scientific Inc).

All solvents were purchased from commercial sources. ^{1}H spectra were recorded using 300 or 400 MHz instruments (Varian), or a 600 MHz instrument (Bruker). Compounds were dissolved in either $CDCl_3$ or DMSO-d_6. Chemical shifts were reported in δ values (parts per million, ppm) and calibrated against solvent peaks δ 2.50 (DMSO-d_6) or δ 7.24 ($CDCl_3$). HRMS was performed by direct injection of compounds dissolved in acetonitrile/water/formic acid (70/29.9/0.1, v/v/v) in to a Q-Exactive mass spectrometer (Thermo) with an electrospray interface, set to positive mode with mass *m/z* = 445.120025 used for internal calibration. All compounds tested were of ≥95 % purity, confirmed by HPLC-DAD with the following instrumentation and conditions: Agilent 1100 series pump and photodiode array detection (180-400 nm), WP Octadocyl column (250 mm length, 4.6 inner diameter, 5 mm particle size) at 22 °C, MeOH/H_20 (75/25, v/v) mobile phase, 1 mL/minute flow rate.

Compounds

Compound 66

To a 100 mL round bottle flask with 5-bromopicolinic acid (7.0 g, 35 mmol) in methanol (80 mL) thionyl chloride (3.0 mL) was added dropwise at room temperature. After addition, the reaction mixture was heated to reflux for 3 h. Methanol was removed and ethyl acetate (100 mL)

was added to the residue and was adjusted pH to 7.0 by addition of sodium bicarbonate solution. The organic phase was separated and dried over sodium sulfate. The organic solvent was removed and methyl 5-bromopicolinate was obtained as white solid (6.57 g, 86.9%), which was used for next step reaction without further purification. A solution of methyl 5-bromopicolinate (6.20 g, 28.7 mmol) in THF anhydrous (150 mL) was added sodium methythionide (2.51 g, 35.9 mmol) and the reaction was heated to reflux for overnight. The solvent was removed and the residue was purified by column chromatography (eluting with hexane and ethyl acetate 1:1). Methyl 5-(methylthio)picolinate as a white solid was isolated (3.0 g, 57.1%): ^{1}H-NMR (300 Hz, $CDCl_3$) δ ppm 8.58 (d, 1H), 8.02 (d, 1H), 7.60 (dd, 1H), 3.99 (s, 3H), 2.58 (s, 3H). To a 100 mL round bottle flask with methyl 5-(methylthio)picolinate **(**1.50 g, 8.2 mmol) in 30 mL of DCM, *m*CPBA (5.51 g, 77%, 25.0 mmol) was added. The reaction was kept at room temperature overnight. After solvent was removed, the residue was purified by column chromatography (eluting with hexane and ethyl acetate 1:1) to give methyl 5-(methylsulfonyl)picolinate as a white solid (1.35g, 76.5%): ^{1}H-NMR (300 Hz, $CDCl_3$) δ ppm 9.22 (d, 1H), 8.40 (dd, 1H), 8.36 (d, 1H), 4.02 (s, 3H), 3.10 (s, 3H). 2-Chloroaniline (1.20 g, 0.0093 mol) in toluene (20 mL) was added trimethylaluminum (2.0 M 4.6 mL) then methyl 5-(methylsulfonyl)picolinate (1.0 g, 4.65 mol) was added and the mixture was heated to 80-90 °C for 2 h. The reaction was cooled down and 1N HCl solution (10 mL) was added for acidification, and dichloromethane (100 mL) was then added. The organic phase was further washed with water (100 mL) and dried over sodium sulfate. The solvent was removed and the residue was mixed with ether (50 mL) and stirred for 0.5 h. The solid was filtered and dried to give N-(2-chlorophenyl)-5-(methylsulfonyl)picolinamide as light yellow solid (1.26 g, 87.2%): ^{1}H-NMR (300 Hz, $CDCl_3$) δ ppm 10.6 (s, 1H), 9.21 (m, 1H), 8.62 (dd, 1H), 8.51 (dd, 1H), 8.46 (dd, 1H), 7.45 (dd, 1H),7.34

(td, 1H), 7.12 (td, 1H), 3.20 (s, 3H). N-(2-chlorophenyl)-5-(methylsulfonyl)picolinamide (1.26 g, 0.0040 mol) in benzene anhydrous (20 mL) was added PCl_5 (1.26 g, 6.0 mmol) and the mixture was heated to reflux for overnight. The solvent was removed and the residue was further dried under high vacuum, and crude N-(2-chlorophenyl)-5-(methylsulfonyl)picolinimidoyl chloride was obtained as a yellow solid (1.60 g). The N-(2-chlorophenyl)-5-(methylsulfonyl)picolinimidoyl chloride was dissolved into THF anhydrous (30 mL) and the reaction was cooled down to 0 °C and hydrazine monohydrate (9.0 mL) was added. The reaction was kept at 0 °C for 10 min and warmed to room temperature in 0.5 h. The solvent was removed and the residue was purified by column chromatography (eluting with hexane and ethyl acetate 1:1) to give N'-(2-chlorophenyl)-5-(methylsulfonyl) picolinimidohydrazide as yellow solid (1.22 g, 92.0 %): ^{1}H-NMR (300 Hz, $CDCl_3$) δ ppm 9.02 (dd, 1H), 8.25 (dd, 1H), 8.17 (dd, 1H) 7.44 (s, 1H), 7.37 (dd, 1H), 7.16 (td, 1H), 6.89 (td, 1H), 6.45 (dd, 1H), 5.62 (s, 2H), 3.06 (s, 3H). In a 100 mL flask with N'-(2-chlorophenyl)-5-(methylsulfonyl) picolinimidohydrazide (0.63 g, 1.94 mol) in toluene anhydrous (20 mL), maleic anhydride (0.20 g, 2.04 mol) was added. The reaction was kept at room temperature for 1 h and then heated to reflux for 3 h. After solvent was removed the residue was dried under high vacuum to give 3-(4-(2-chlorophenyl)-5-(5-(methylsulfonyl)pyridin-2-yl)-4H-1,2,4-triazol-3-yl)acrylic acid as yellow solid (0.75 g, 95.6%). To a solution of 4-Cyano-benzoic acid methyl ester (1.0 g, 13 mmol) in 30 mL of methanol, 3 mL of $H_2NNH_2{\cdot}H_2O$ was added. The mixture was stirred at room temperature for 16 h. The solid was collected and washed with methanol to give 4-Cyano-benzoic acid hydrazide as a solid (0.8 g, 80%): ^{1}HNMR (DMSO-d_6): δ ppm 7.93 (d, 4 H); 4.70 (s, 1 H); 3.30 (s, 2 H). In a 100 mL flask with 3-(4-(2-chlorophenyl)-5-(5-(methylsulfonyl)pyridin-2-yl)-4H-1,2,4-triazol-3-yl)acrylic acid (0.21 g, 0.52 mmol) in dichlormethane (20 mL), oxalyl chloride (0.20 g, 1.55 mmol) and a

drop of DMF were added. The reaction was kept at room temperature for 3 h. The solvent was removed and the residue was further dried under high vacuum and cooled to -20 °C. Dichlormethane (10 mL) was added, followed by 4-cyanobenzohydrazide (0.10 mg, 0.62 mmol) and triethylamine (0.5 mL). The reaction was kept at this temperature for 0.5 h and then room temperature for 1 h. The solvent was removed and the resulting crude (E)-N'-(3-(4-(2-chlorophenyl)-5-(5-(methylsulfonyl)pyridin-2-yl)-4H-1,2,4-triazol-3-yl)acryloyl)-4-cyanobenzohydrazide was used for next step. (E)-N'-(3-(4-(2-chlorophenyl)-5-(5-(methylsulfonyl)pyridin-2-yl)-4H-1,2,4-triazol-3-yl)acryloyl)-4-cyanobenzohydrazide was dissolved into dichlormethane (10 mL), and was added triphenyl phosphine (0.27 g, 1.0 mmol), carbon tetrabromide (0.34 g, 1.04 mmol) and triethylamine (0.18 mL, 1.30 mmol). The reaction was kept at room temperature for 2 h. The final compound was purified by column chromatography (eluting with hexane and ethyl acetate 1:3) to give (E)-4-(5-(2-(4-(2-chlorophenyl)-5-(5-(methylsulfonyl)pyridin-2-yl)-4H-1,2,4-triazol-3-yl)vinyl)-1,3,4-oxadiazol-2-yl)benzonitrile.

66, lead compound: Mp: 257-259°C; TLC ($CHCl_3$: MeOH, 90:10 v/v): $R_f = 0.60$; UV/Vis: λ_{max} 323 nm. ^{1}H NMR (600 MHz, DMSO-*d6*): δ 8.73 (dd, *J* = 2.3 Hz, 0.8 Hz, 1H), 8.53 (dd, *J* = 8.3 Hz, 0.8 Hz, 1H), 8.47 (dd, *J* = 8.4 Hz, 2.3 Hz, 1H), 8.20 (m, 2H), 8.08 (m, 2H), 7.83-7.80 (m, 2H), 7.73-7.70 (m, 1H), 7.63 (dt, *J* = 6.7 Hz, 1.4 Hz, 1H), 7.45 (d, *J* = 16.4 Hz, 1H), 7.13 (d, *J* = 16.8 Hz, 1H), 3.35 (s, *J* = 6.99 Hz, 3H). ^{13}C NMR (600MHz, DMSO-d_6): δ 163.6, 163.5, 152.8, 152.5, 149.8, 147.9, 137.8, 137.1, 134.1, 133.8, 132.6, 132.5, 131.4, 130.7, 130.4, 129.2, 128.4, 128.0, 127.4, 123.8, 121.2, 118.5, 117.0, 114.7, 15.61. HRMS (*m*/*z*): [MH]+ calcd. for $C_{25}H_{17}ClN_7O_3S^+$, 530.08; found, 530.08.

1, starting molecule**:** Mp: 169-171°C; TLC ($CHCl_3$: MeOH, 90:10 v/v): R_f =0.59; UV/Vis: λ_{max} 230, 251 nm. ^{1}H NMR (600 MHz, $CDCl_3$): δ 8.55 (d, *J* = 6.2 Hz, 2H); 7.90 (d, *J* = 4.5 Hz, 2H); 7.32 (d, *J* = 6.2 Hz, 2H); 7.25 (d, *J* = 4.5 Hz, 2H); 7.15 (d, *J* = 8.96 Hz, 2H); 6.99 (d, *J* = 8.96 Hz, 2H); 4.73 (s, 1H); 3.85 (s, 1H); 2.39 (s, 1H). ^{13}C NMR (600MHz, $CDCl_3$): δ 174.8, 168.7, 161.0, 153.2, 152.4, 150.3, 141.8, 133.8, 129.6, 128.3, 127.4, 125.5, 123.5, 121.4, 115.5, 55.6, 41.0, 26.9, 21.6. HRMS (*m*/*z*): [MH]+ calcd. For $C_{25}H_{23}N_6O_2S^+$, 471.16; found, 471.14.

Plasmids, constructs, cell lines and conditioned media

The L Wnt3a-expressing cells were purchased from ATCC (American Type Culture Collection) and, including ST-Luc/Ren HEK293 cells (see below), maintained according to the supplier's recommendations. A stable HEK293 cell line containing SuperTOP-Flash plasmid (ST-Luc HEK293) (7 X TCF binding sites promoter)[52] was kindly provided by V. Korinek. To create SuperTOP-Luciferase/Renilla HEK293 cells (ST-Luc/Ren HEK293), the pRL-TK (*Renilla*, Promega) cassette was subcloned into pPUR (Promega) giving rise to the construct pRL-TK-puro. Linearized pRL-TK-puro was transfected (FuGENE6, Roche) into ST-Luc HEK293 before selection (2.5 µg/mL Puromycin, Sigma). Wnt3a containing conditioned media (Wnt3a-CM) from L Wnt3a expressing cells was collected as described by ATCC.

Transfection and luciferase assays

40,000 ST-Luc/Ren HEK293 cells were seeded in 96-well plates coated with poly-L lysine. 24 hours after seeding, the cells were incubated for an additional 24 hours with various compound concentrations in 50 % Wnt3a-CM. After compound exposures, the cells were lysed

and the firefly luciferase and *Renilla* activities were measured on a GloMax® Luminometer (Promega) using Dual-Glo Luciferase Assay System (Promega).

TNKS1, TNKS2 and PARP1 *in vitro* biochemical assays

66 inhibitory activity at various doses (duplicates) was tested twice against TNKS1 (80564), TNSK2 (80576) and PARP1 (80551) Chemiluminescent Assay Kits (BPS Bioscience, Nordic Biosite). The procedures were performed according to the protocols from BPS Bioscience and the luminescence was measured on a GloMax® Luminometer (Promega).

IC50 calculations

XLfit (idbs) was used to determine the IC50-values in inhibition experiments. The following formula was chosen to fit the data points (Langmuir Binding Isotherm):

fit = ((A+(B*x))+(((C-B)*(1-exp((-1*D)*x)))/D)), res = (y-fit)

HLM analysis

The human liver microsome analysis (HLM) was performed according to the standard protocols of Medicilon/MPI Preclinical Research (Shanghai, China) or Cyprotex (Macclesfield, United Kingdom).

Chemoproteomics target profiling assay

Chemoproteomics target profiling assays were carried out as described previously[30] with minor modifications: Compound 161 was immobilized on sepharose resin and the affinity matrix was washed in lysis buffer. Aliquots of HEK293 cell lysate (5 mg total protein each) were pre-

incubated with 20 μM of the tankyrase inhibitor **66** or the inactive **25** (all containing 1% DMSO) or with vehicle control at 4 °C. 35 μL 161 affinity matrix per sample was added and incubated for two hours, before being washed extensively and eluted. Separation of eluted proteins by SDS-PAGE, processing of gels, labeling with TMT tags (Thermo-Fisher Scientific), LC-MS/MS analysis on a nano-LC system (Eksigent 1D+) coupled to an LTQ-Orbitrap Velos mass spectrometer (Thermo Fisher Scientific) and peptide and protein identification were all done as described.[30]

Reporter ion intensity for the vehicle control was defined as 0% competition. A protein competed to a larger extend than defined by the 3 times standard deviation interval was considered to be specifically bound. Competition data was analyzed and plotted using Tableau software.

Kinase, phosphatase and GPCR assays

The kinase, phosphatase and GPCR assays were performed as described in KinaseProfiler™ Service and GPCRProfiler® Assay Protocols (Millipore).

Modeling of metabolic stability in human liver microsomes

During synthesis of new compounds two types of *in silico* approaches were used: Ranking of sites of metabolism (SOM) in cytochromes P450 and estimation of half-life times in human liver microsomes. Five software packages, based on different approaches, have been used in the study: MetaPrint2D, SmartCYP 2.3, MetaDrug, MetaSite 3.1.2 and SOME 1.3.[35-39] Each program calculated the individual scores for non-hydrogen atoms. The top three calculated SOM atoms were used in SOM consensus score calculations. Descending rank values were assigned to

each of the top three predicted SOMs (from most unstable to least unstable): 3 for the first SOM, 2 for the second SOM and 1 for the third SOM.

A second *in silico* approach was used to evaluate a quantitative correlation between *in silico* predictions and metabolism in human liver microsomes. The programs used estimated metabolic stability against members of the cytochrome P450 family. We hypothesized that an overall metabolic stability in HLM assays correlates with the scores of the highest ranked SOMs as these atoms are supposed to kinetically define the fastest metabolism reaction. This correlation was observed with all programs except Metadrug. The metabolism rate consensuses scores (MRCS), based on the first site of metabolism from each program, were estimated by the following formula:

$$MRCS = \frac{\text{SmartCyp Score}}{\text{avg(SmartCyp Score)}} \times \frac{\text{avg(MetaSite score)}}{\text{MetaSite score}} \times \frac{\text{MetaPrint2D score}}{\text{avg(MetaPrint2D score)}} \times \frac{\text{avg(SOME score)}}{\text{SOME score}}$$

Predictions of metabolic modifications

Three software packages were used in the analysis and identification of metabolic top SOMs: MetaDrug, MetaSite 3.1.2 and SOME 1.3. The main metabolic reactions were suggested by all three programs: Oxidation of sulfur, N-oxidation of nitrogen in position 4 of region E, O-dealkylation of methoxy groups, aliphatic hydroxylations of carbons in region C and in the methyl group of region A. The aromatic hydroxylation was predicted as a metabolism reaction for the aromatic carbons. MetaDrug and MetaSite prediced dealkylation of the sulfur by breaking a bond between carbon and sulfur in the region C in addition to oxidation.

Optimization of cytochromes P450 inhibition

LogP calculations were performed using the program ALOGP2.1. The program calculates average LogP values based on several methods along with standard deviation estimations.[33, 34]

Pharmacokinetical analysis

The pharmacokinetical (PK) analyses, per oral injections (p.o.), intra peritoneal (i.p.) and intravenous injections (i.v.) were performed according to the standard protocols of Medicilon/MPI Preclinical Research Shanghai, China. A total of 160 male and female ICR mice from Sino-British SIPPR/BK Lab Animal Ltd, Shanghai (18.2-26.0 grams) were used in the study. The feed were provided *ad libitum* throughout the in-life portion with the exception of the overnight fasting period (10-15 hours) prior to oral administration. **66** was administered via intravenous injection (i.v.) or oral administration (p.o.) or intraperitoneal injection (i.p.), respectively. The i.v. and i.p formulations were made in 5% DMSO, 50% PEG400, 45% saline. The p.o. formulation was made in 10% NMP, 60% PEG400, 30% saline. Blood samples (approximately 500 μL) were collected via cardiac puncture after euthanasia by carbon dioxide inhalation at 5 min, 15 min, 30 min, 1, 2, 4, 8, and 24 hours post dose. Blood samples were placed into tubes containing sodium heparin and centrifuged at 8000 rpm for 6 minutes at 4°C to separate plasma from the samples. Analyses of the plasma samples were conducted by the Analytical Sciences Division of Medicilon Preclinical Research (Shanghai) LLC. The concentrations of **66** in plasma were determined using a high performance liquid chromatography/mass spectrometry (HPLC-MS/MS). No interfering peaks were detected at the

retention time of the analyte or the IS indicating that the method was specific for both **66** and the IS.

Crystallography, Transformation and expression

Plasmid pNIC-Bsa4 contains the catalytic PARP-domain of human tankyrase 2 (L_{940} – G_{1162}) with an N-terminal His_6 tag. The plasmid was transformed into *E. coli* Rosetta II. Colonies were inoculated in LB medium over night (o/n) at 37 ˚C, 200 rpm, containing 35 µg/mL CAM and 50 µg/mL KAN. Fresh o/n cultures were used to inoculate 1 L TB medium supplemented with 35 µg/mL CAM, 50 µg/mL KAN and 130 µL antifoam (addition of 100 phosphate buffer to TB medium was added the same day (to keep it sterile for as long as possible)). The culture was grown at 37 ˚C, 200 rpm until OD_{600} reached ~1.5. The culture was down-tempered to room-temperature and expression of the catalytic PARP-domain of TNKS2 was induced by addition of 0.5 mM IPTG and growth continued overnight at 18 ˚C, with full airflow in a Lex Harbinger Fermentor. Cells were harvested by centrifugation at 6,000 x g for 30 min, 4 ˚C. The resulting cell pellet was resuspended in resolubilization buffer (50 mM Tris-HCl, 5 % glycerol) supplemented with 1 mM freshly added PMSF, distributed into 50 mL tubes, and centrifuged at 4000 rpm for 15 min, 4 ˚C. Cell pellets were stored at -20 ˚C until further use.

Crystallography, Extraction and purification

A 10 times weight volume lysis buffer (30 mM Tris-HCl (pH 7.6), 300 mM NaCl, 10% glycerol, 0.5 mM DTT and 10 mM imidazole) supplemented with 1 mM PMSF and 1 µg/mL DNAse was added to 17-22 g wet weight of cells. Cells were lysed using a High Pressure Homogenizer C3 (Avestin) at a pressure between 1000 and 1500 bar. Cell debris was removed

by centrifugation at 18,000 rpm for 35 minutes, 4 ˚C. Protein purification was performed using ÄKTAprime Plus (for IMAC) and ÄKTApurifier (GE Healthcare). Prior to purification, IMAC column was equilibrated using wash buffer 1 (30 mM Tris-HCl, 500 mM NaCl, 10 % glycerol, 10 mM imidazole and 0.5 mM DTT.

The lysate was loaded onto the column, usually at a volume of 200 mL and run through the column once or twice at 4-5 ml/min. The column was then washed with wash buffer 1 (2-3 V_{COL}) followed by wash buffer 2 (30 mM Tris-HCl, 500 mM NaCl, 10% glycerol, 25 mM imidazole and 0.5 mM DTT) (~5 V_{COL}). Bound protein was eluted with IMAC elution buffer (30 mM Tris-HCl, 500 mM NaCl, 10% glycerol, 500 mM imidazole and 0.5 mM DTT) at a flow rate of 4-5 ml/min in 5 mL fractions. The 5 ml-fractions were analyzed by SDS-PAGE. Target fraction was pooled and concentrated down to 1 mL before applied to the GF column (30 mM Tris-HCl, 300 mM NaCl, 10% glycerol and 0.5 mM DTT). Fresh DTT was added at a final concentration of 2 mM. Purified protein was analyzed again using SDS-PAGE and target fraction was concentrated to 20-30 mg/mL using a VivaSpin 6 10,000 MWCO centrifugal filter device (Sartorius Stedim Biotech). Concentration was measured using the NanoDrop 2000 Spectrophotometer, 1:10 dilutions (Thermo Scientific). Protein solution was flash-freezed with liquid nitrogen and stored at – 80 ˚C until further use.

Crystallography, Crystallization

Crystals were obtained by the sitting drop vapor diffusion method in a 24-well plate. A volume of 1 µL protein solution, including **66** at a ratio 10:1 (ligand:protein), was dissolved at 60 ˚C, 5 min and resuspended by vortexing. 1 µL of a 0.15 M **66** solution was added to a 50 µL protein solution concentrated to 15 mg/mL and left to incubate 10 min on ice. The protein: **66**

solution was mixed 1:1 with the well solution (100 mM NaOAc pH 4.5 and 16-26% PEG 3350). All steps were performed in the cold room. The plates were left to incubate at 4 ˚C. Crystals appeared after ~ 1 week and continued to grow for ≥ 2 weeks more. Crystals were quickly transferred to a cryo solution containing 30% ethylene glycol mixed with reservoir solution and frozen in liquid nitrogen.

The TNKS2$^{946-1162}$ domain is highly temperature sensitive in the presence of **66** and had to be kept cold throughout the entire procedure crystallization setup. Heavy precipitate (**66**) was observed immediately in the presence of the crystallization conditions. Crystals only appeared when the protein concentration was above 15 mg/mL. It was usually necessary to add additional glycerol in the reservoir chamber to push the vapor diffusion experiment further. Compared to Karlberg and coworkers,[47] it was not necessary to use an *in situ* proteolysis crystallization strategy.

Crystallography, Data collection and refinement

Diffraction data were collected at 100 K on the end stations X06DA at the Swiss Light Source (SLS). The diffraction data were processed and scaled with XDS.[53] Phases were obtained by molecular replacement using the program PHASER[54] and a search model of the tankyrase 2 PARP domain (PDB ID 3MHJ).[24] Model building was performed using Coot[55] and model refinement was performed with phenix.refine.[56] For reflection file handling, programs from the CCP4 package were used.[57] All structural figures in this paper were prepared with Pymol (http://www.pymol.org). The atomic coordinates and experimental data (code 4HYF) have been deposited in the Protein Data Bank.

Bioinformatics and alignment of the human PARP domains were performed with default settings in MAFFT[58] and edited by hand in Jalview.[59]

ACKNOWLEDGMENT

This work was supported by the CRI program of the Research Council of Norway, and by Helse Sør Øst, grant 2010031. We thank TC Scientific Inc for excellent compound synthesis and Marcus Bantscheff for protein mass spectrometry during affinity-capture experiments. We thank Herwig Schuler for providing expression plasmids and information needed for the production of recombinant proteins. The authors also wish to express gratitude for beam line support by the staff at the (Swiss Light Source) and the Berliner Elektronenspeicherring-Gesellschaft fur Synchrotronstrahlung (BESSY) for making our experiments possible. Initial crystal tests and opmtimization was performed at BESSY. A special thanks to the Blix foundation for supporting the laboratory with additional equipment to finish the study.

ANCILLARY INFORMATION

Supporting Information Available: Supplementary Figures and Chemistry. This material is available free of charge via the Internet at http://pubs.acs.org.

REFERENCES

(1) Hottiger, M. O.; Hassa, P. O.; Luscher, B.; Schuler, H.; Koch-Nolte, F. Toward a unified nomenclature for mammalian ADP-ribosyltransferases. *Trends Biochem. Sci.* **2010,** *35*, 208-219.

(2) Guettler, S.; LaRose, J.; Petsalaki, E.; Gish, G.; Scotter, A.; Pawson, T.; Rottapel, R.; Sicheri, F. Structural basis and sequence rules for substrate recognition by Tankyrase explain the basis for cherubism disease. *Cell* **2011,** *147*, 1340-1354.

(3) Hsiao, S. J.; Smith, S. Tankyrase function at telomeres, spindle poles, and beyond. *Biochimie* **2008,** *90*, 83-92.

(4) Sbodio, J. I.; Chi, N. W. Identification of a tankyrase-binding motif shared by IRAP, TAB182, and human TRF1 but not mouse TRF1. NuMA contains this RXXPDG motif and is a novel tankyrase partner. *J. Biol. Chem.* **2002,** *277*, 31887-31892.

(5) Seimiya, H.; Smith, S. The telomeric poly(ADP-ribose) polymerase, tankyrase 1, contains multiple binding sites for telomeric repeat binding factor 1 (TRF1) and a novel acceptor, 182-kDa tankyrase-binding protein (TAB182). *J. Biol. Chem.* **2002,** *277*, 14116-14126.

(6) Seimiya, H.; Muramatsu, Y.; Smith, S.; Tsuruo, T. Functional subdomain in the ankyrin domain of tankyrase 1 required for poly(ADP-ribosyl)ation of TRF1 and telomere elongation. *Mol. Cell Biol.* **2004,** *24*, 1944-1955.

(7) De Rycker M.; Price, C. M. Tankyrase polymerization is controlled by its sterile alpha motif and poly(ADP-ribose) polymerase domains. *Mol. Cell Biol.* **2004,** *24*, 9802-9812.

(8) Ha, G. H.; Kim, H. S.; Go, H.; Lee, H.; Seimiya, H.; Chung, D. H.; Lee, C. W. Tankyrase-1 function at telomeres and during mitosis is regulated by Polo-like kinase-1-mediated phosphorylation. *Cell Death. Differ.* **2012,** *19*, 321-332.

(9) Smith, S.; Giriat, I.; Schmitt, A.; de Lange, T. Tankyrase, a poly(ADP-ribose) polymerase at human telomeres. *Science* **1998,** *282*, 1484-1487.

(10) Chi, N. W.; Lodish, H. F. Tankyrase is a golgi-associated mitogen-activated protein kinase substrate that interacts with IRAP in GLUT4 vesicles. *J. Biol. Chem.* **2000,** *275*, 38437-38444.

(11) Guo, H. L.; Zhang, C.; Liu, Q.; Li, Q.; Lian, G.; Wu, D.; Li, X.; Zhang, W.; Shen, Y.; Ye, Z.; Lin, S. Y.; Lin, S. C. The Axin/TNKS complex interacts with KIF3A and is required for insulin-stimulated GLUT4 translocation. *Cell Res.* **2012,** *22*, 1246-1257.

(12) Chang, P.; Coughlin, M.; Mitchison, T. J. Interaction between Poly(ADP-ribose) and NuMA contributes to mitotic spindle pole assembly. *Mol. Biol. Cell* **2009,** *20*, 4575-4585.

(13) Ozaki, Y.; Matsui, H.; Asou, H.; Nagamachi, A.; Aki, D.; Honda, H.; Yasunaga, S.; Takihara, Y.; Yamamoto, T.; Izumi, S.; Ohsugi, M.; Inaba, T. Poly-ADP ribosylation of Miki by tankyrase-1 promotes centrosome maturation. *Mol. Cell* **2012,** *47*, 694-706.

(14) Kim, I. K.; Kiefer, J. R.; Ho, C. M.; Stegeman, R. A.; Classen, S.; Tainer, J. A.; Ellenberger, T. Structure of mammalian poly(ADP-ribose) glycohydrolase reveals a flexible tyrosine clasp as a substrate-binding element. *Nat. Struct. Mol. Biol.* **2012,** *19*, 653-656.

(15) Levaot, N.; Voytyuk, O.; Dimitriou, I.; Sircoulomb, F.; Chandrakumar, A.; Deckert, M.; Krzyzanowski, P. M.; Scotter, A.; Gu, S.; Janmohamed, S.; Cong, F.; Simoncic, P. D.; Ueki, Y.; La Rose, J.; Rottapel, R. Loss of Tankyrase-mediated destruction of 3BP2 is the underlying pathogenic mechanism of cherubism. *Cell* **2011,** *147*, 1324-1339.

(16) Huang, S. M.; Mishina, Y. M.; Liu, S.; Cheung, A.; Stegmeier, F.; Michaud, G. A.; Charlat, O.; Wiellette, E.; Zhang, Y.; Wiessner, S.; Hild, M.; Shi, X.; Wilson, C. J.; Mickanin, C.; Myer, V.; Fazal, A.; Tomlinson, R.; Serluca, F.; Shao, W.; Cheng, H.; Shultz, M.; Rau, C.;

Schirle, M.; Schlegl, J.; Ghidelli, S.; Fawell, S.; Lu, C.; Curtis, D.; Kirschner, M. W.; Lengauer, C.; Finan, P. M.; Tallarico, J. A.; Bouwmeester, T.; Porter, J. A.; Bauer, A.; Cong, F. Tankyrase inhibition stabilizes axin and antagonizes Wnt signalling. *Nature* **2009,** *461*, 614-620.

(17) Waaler, J.; Machon, O.; Tumova, L.; Dinh, H.; Korinek, V.; Wilson, S. R.; Paulsen, J. E.; Pedersen, N. M.; Eide, T. J.; Machonova, O.; Gradl, D.; Voronkov, A.; von Kries, J. P.; Krauss, S. A novel tankyrase inhibitor decreases canonical Wnt signaling in colon carcinoma cells and reduces tumor growth in conditional APC mutant mice. *Cancer Res.* **2012,** *72*, 2822-2832.

(18) Callow, M. G.; Tran, H.; Phu, L.; Lau, T.; Lee, J.; Sandoval, W. N.; Liu, P. S.; Bheddah, S.; Tao, J.; Lill, J. R.; Hongo, J. A.; Davis, D.; Kirkpatrick, D. S.; Polakis, P.; Costa, M. Ubiquitin ligase RNF146 regulates tankyrase and Axin to promote Wnt signaling. *PLoS. One.* **2011,** *6*, e22595.

(19) Zhang, Y.; Liu, S.; Mickanin, C.; Feng, Y.; Charlat, O.; Michaud, G. A.; Schirle, M.; Shi, X.; Hild, M.; Bauer, A.; Myer, V. E.; Finan, P. M.; Porter, J. A.; Huang, S. M.; Cong, F. RNF146 is a poly(ADP-ribose)-directed E3 ligase that regulates axin degradation and Wnt signalling. *Nat. Cell Biol.* **2011,** *13*, 623-629.

(20) Bao, R.; Christova, T.; Song, S.; Angers, S.; Yan, X.; Attisano, L. Inhibition of tankyrases induces axin stabilization and blocks wnt signalling in breast cancer cells. *PLoS. One.* **2012,** *7*, e48670.

(21) Casas-Selves, M.; Kim, J.; Zhang, Z.; Helfrich, B. A.; Gao, D.; Porter, C. C.; Scarborough, H. A.; Bunn, P. A., Jr.; Chan, D. C.; Tan, A. C.; Degregori, J. Tankyrase and the canonical Wnt pathway protect lung cancer cells from EGFR inhibition. *Cancer Res.* **2012**.

(22) Kirby, C. A.; Cheung, A.; Fazal, A.; Shultz, M. D.; Stams, T. Structure of human tankyrase 1 in complex with small-molecule inhibitors PJ34 and XAV939. *Acta Crystallogr. Sect. F. Struct. Biol. Cryst. Commun.* **2012,** *68*, 115-118.

(23) Gunaydin, H.; Gu, Y.; Huang, X. Novel binding mode of a potent and selective tankyrase inhibitor. *PLoS. One.* **2012,** *7*, e33740.

(24) Wahlberg, E.; Karlberg, T.; Kouznetsova, E.; Markova, N.; Macchiarulo, A.; Thorsell, A. G.; Pol, E.; Frostell, A.; Ekblad, T.; Oncu, D.; Kull, B.; Robertson, G. M.; Pellicciari, R.; Schuler, H.; Weigelt, J. Family-wide chemical profiling and structural analysis of PARP and tankyrase inhibitors. *Nat. Biotechnol.* **2012,** *30*, 283-288.

(25) Waaler, J.; Machon, O.; Holsworth, D.; Krauss, S. Azole derivates as Wnt pathway inhibitors. International application number: PCT/GB2010/001118, International publication number: WO 2010/139966 A1. 12-9-2010.

(26) Waaler, J.; Machon, O.; von Kries, J. P.; Wilson, S. R.; Lundenes, E.; Wedlich, D.; Gradl, D.; Paulsen, J. E.; Machonova, O.; Dembinski, J. L.; Dinh, H.; Krauss, S. Novel synthetic antagonists of canonical Wnt signaling inhibit colorectal cancer cell growth. *Cancer Res.* **2011,** *71*, 197-205.

(27) Chen, B.; Dodge, M. E.; Tang, W.; Lu, J.; Ma, Z.; Fan, C. W.; Wei, S.; Hao, W.; Kilgore, J.; Williams, N. S.; Roth, M. G.; Amatruda, J. F.; Chen, C.; Lum, L. Small molecule-mediated disruption of Wnt-dependent signaling in tissue regeneration and cancer. *Nat. Chem. Biol.* **2009,** *5*, 100-107.

(28) Narwal, M.; Venkannagari, H.; Lehtio, L. Structural basis of selective inhibition of human tankyrases. *J. Med. Chem.* **2012,** *55*, 1360-1367.

(29) Waaler, J.; Machon, O.; Voronkov, A.; Holsworth, D.; Krauss, S. Triazole derivatives as Wnt signaling pathway inhibitors. International application number: PCT/GB2011/05244, International patent number: WO 2012/076898 A1. 6-14-2012.

(30) Bantscheff, M.; Hopf, C.; Savitski, M. M.; Dittmann, A.; Grandi, P.; Michon, A. M.; Schlegl, J.; Abraham, Y.; Becher, I.; Bergamini, G.; Boesche, M.; Delling, M.; Dumpelfeld, B.; Eberhard, D.; Huthmacher, C.; Mathieson, T.; Poeckel, D.; Reader, V.; Strunk, K.; Sweetman, G.; Kruse, U.; Neubauer, G.; Ramsden, N. G.; Drewes, G. Chemoproteomics profiling of HDAC inhibitors reveals selective targeting of HDAC complexes. *Nat. Biotechnol.* **2011,** *29*, 255-265.

(31) Bisht, K. K.; Dudognon, C.; Chang, W. G.; Sokol, E. S.; Ramirez, A.; Smith, S. GDP-mannose-4,6-dehydratase is a cytosolic partner of tankyrase 1 that inhibits its poly(ADP-ribose) polymerase activity. *Mol. Cell Biol.* **2012,** *32*, 3044-3053.

(32) Moriwaki, K.; Shinzaki, S.; Miyoshi, E. GDP-mannose-4,6-dehydratase (GMDS) deficiency renders colon cancer cells resistant to tumor necrosis factor-related apoptosis-inducing ligand (TRAIL) receptor- and CD95-mediated apoptosis by inhibiting complex II formation. *J. Biol. Chem.* **2011,** *286*, 43123-43133.

(33) Tetko, I. V.; Gasteiger, J.; Todeschini, R.; Mauri, A.; Livingstone, D.; Ertl, P.; Palyulin, V. A.; Radchenko, E. V.; Zefirov, N. S.; Makarenko, A. S.; Tanchuk, V. Y.; Prokopenko, V. V. Virtual computational chemistry laboratory--design and description. *J. Comput. Aided Mol. Des* **2005,** *19*, 453-463.

(34) Tetko, I. V.; Poda, G. I.; Ostermann, C.; Mannhold, R. Large-scale evaluation of log P predictors: local corrections may compensate insufficient accuracy and need of experimentally testing every other compound. *Chem. Biodivers.* **2009,** *6*, 1837-1844.

(35) Carlsson, L.; Spjuth, O.; Adams, S.; Glen, R. C.; Boyer, S. Use of historic metabolic biotransformation data as a means of anticipating metabolic sites using MetaPrint2D and Bioclipse. *BMC. Bioinformatics.* **2010,** *11*, 362.

(36) Cruciani, G.; Carosati, E.; De Boeck, B.; Ethirajulu, K.; Mackie, C.; Howe, T.; Vianello, R. MetaSite: understanding metabolism in human cytochromes from the perspective of the chemist. *J. Med. Chem.* **2005,** *48*, 6970-6979.

(37) Ekins, S.; Bugrim, A.; Brovold, L.; Kirillov, E.; Nikolsky, Y.; Rakhmatulin, E.; Sorokina, S.; Ryabov, A.; Serebryiskaya, T.; Melnikov, A.; Metz, J.; Nikolskaya, T. Algorithms for network analysis in systems-ADME/Tox using the MetaCore and MetaDrug platforms. *Xenobiotica* **2006,** *36*, 877-901.

(38) Rydberg, P.; Gloriam, D. E.; Olsen, L. The SMARTCyp cytochrome P450 metabolism prediction server. *Bioinformatics.* **2010,** *26*, 2988-2989.

(39) Zheng, M.; Luo, X.; Shen, Q.; Wang, Y.; Du, Y.; Zhu, W.; Jiang, H. Site of metabolism prediction for six biotransformations mediated by cytochromes P450. *Bioinformatics.* **2009,** *25*, 1251-1258.

(40) Topliss, J. G. Utilization of operational schemes for analog synthesis in drug design. *J. Med. Chem.* **1972,** *15*, 1006-1011.

(41) Chauret, N.; Guay, D.; Li, C.; Day, S.; Silva, J.; Blouin, M.; Ducharme, Y.; Yergey, J. A.; Nicoll-Griffith, D. A. Improving metabolic stability of phosphodiesterase-4 inhibitors containing a substituted catechol: prevention of reactive intermediate formation and covalent binding. *Bioorg. Med. Chem. Lett.* **2002,** *12*, 2149-2152.

(42) Shultz, M. D.; Kirby, C. A.; Stams, T.; Chin, D. N.; Blank, J.; Charlat, O.; Cheng, H.; Cheung, A.; Cong, F.; Feng, Y.; Fortin, P. D.; Hood, T.; Tyagi, V.; Xu, M.; Zhang, B.; Shao, W.

[1,2,4]triazol-3-ylsulfanylmethyl)-3-phenyl-[1,2,4]oxadiazoles: antagonists of the Wnt pathway that inhibit tankyrases 1 and 2 via novel adenosine pocket binding. *J. Med. Chem.* **2012,** *55*, 1127-1136.

(43) Miteva, M. A.; Guyon, F.; Tuffery, P. Frog2: Efficient 3D conformation ensemble generator for small compounds. *Nucleic Acids Res.* **2010,** *38*, W622-W627.

(44) Meslamani, J. E.; Andre, F.; Petitjean, M. Assessing the geometric diversity of cytochrome P450 ligand conformers by hierarchical clustering with a stop criterion. *J. Chem. Inf. Model.* **2009,** *49*, 330-337.

(45) Craig P.N. Interdependence between physical parameters and selection of substituent groups for correlation studies. Aug;14(8):680-4. *J Med Chem.* **1971,** *14(8)*, 680-684.

(46) Craig P.N. Structure-activity correlations of antimalarial compounds. 1. Free-Wilson analysis of 2-phenylquinoline-4-carbinols. *J Med Chem* **1972,** 144-149.

(47) Karlberg, T.; Markova, N.; Johansson, I.; Hammarstrom, M.; Schutz, P.; Weigelt, J.; Schuler, H. Structural basis for the interaction between tankyrase-2 and a potent Wnt-signaling inhibitor. *J. Med. Chem.* **2010,** *53*, 5352-5355.

(48) Personal Communication, Herwig Schuler. 2013.

(49) Mosca, R.; Schneider, T. R. RAPIDO: a web server for the alignment of protein structures in the presence of conformational changes. *Nucleic Acids Res.* **2008,** *36*, W42-W46.

(50) Lehtio, L.; Collins, R.; van den, B. S.; Johansson, A.; Dahlgren, L. G.; Hammarstrom, M.; Helleday, T.; Holmberg-Schiavone, L.; Karlberg, T.; Weigelt, J. Zinc binding catalytic domain of human tankyrase 1. *J. Mol. Biol.* **2008,** *379*, 136-145.

(51) Fitzgerald, C. E.; Patel, S. B.; Becker, J. W.; Cameron, P. M.; Zaller, D.; Pikounis, V. B.; O'Keefe, S. J.; Scapin, G. Structural basis for p38alpha MAP kinase quinazolinone and pyridol-pyrimidine inhibitor specificity. *Nat. Struct. Biol.* **2003,** *10*, 764-769.

(52) Veeman, M. T.; Slusarski, D. C.; Kaykas, A.; Louie, S. H.; Moon, R. T. Zebrafish prickle, a modulator of noncanonical Wnt/Fz signaling, regulates gastrulation movements. *Curr. Biol.* **2003,** *13*, 680-685.

(53) Kabsch, W. Automatic Processing of Rotation Diffraction Data from Crystals of Initially Unknown Symmetry and Cell Constants. *Journal of applied Crystallography* **1993,** *26*, 795-800.

(54) McCoy A.J.; Grosse-Kunstleve R.W.; Storoni L.C.; Read R.J. Likelihood-enhanced fast translation functions. *Acta Crystallogr. D Biol. Crystallogr.* **2005,** *61*, 458-464.

(55) Emsley P.; Cowtan K. Coot: model-building tools for molecular graphics. *Acta Crystallogr. D Biol. Crystallogr.* **2004,** *60*, 2126-2132.

(56) Afonine, P. V.; Grosse-Kunstleve, R. W.; Adams, P. D. The Phenix refinement framework. *CCP4 Newsletter on protein crystallography* **2005,** *42*, Contribution 8.

(57) The CCP4 suite: programs for protein crystallography. *Acta Crystallogr. D. Biol. Crystallogr.* **1994,** *50*, 760-763.

(58) Katoh, K.; Misawa, K.; Kuma, K.; Miyata, T. MAFFT: a novel method for rapid multiple sequence alignment based on fast Fourier transform. *Nucleic Acids Res.* **2002,** *30*, 3059-3066.

(59) Clamp, M.; Cuff, J.; Searle, S. M.; Barton, G. J. The Jalview Java alignment editor. *Bioinformatics.* **2004,** *20*, 426-427.

FIGURE LEGENDS

Figure 1. Mapping of sub-proteomes binding to the **24** probe matrix. (a) Chemical structures of the immobilized active compound (**24**), the active competitor (**66**) and the inactive compound (**25**). (b) Scatter plot depicting all quantified proteins (n=168) in a 3-channel TMT quantitative chemical proteomics experiment. Proteins, each represented by a square, are plotted as a function of the % competition with the active compound **66** relative to the vehicle DMSO (y-axis) and versus the % competition with the inactive compound **25** relative to DMSO (x-axis). The yellow lines indicate three standard deviations (threshold) from the average competition value across all quantified proteins. All proteins that are specifically competed with the active compound are highlighted in red. (c) The graphs show the biochemical IC_{50}-values of **66** against TNKS1 (dark grey), TNKS2 (black) or PARP1 (light grey). In biochemical assays, **66** specifically inhibits TNKS1 and TNKS2 but not PARP1. The x-axis is shown with a logarithmic (log) scale. The mean values represent minimum two independent experiments and the error bars show standard deviations (s.d.). Calculated IC_{50}-values are displayed in table along with error estimations (s.d.).

Figure 2. (a) Selected key chemical structures of the SAR leading to **66**. **1** (upper left panel) is dissected into specific regions (A-E) of evaluation/chemical modification. **66** is a RO5 compliant, potent, stable, selective TNKS1/2 inhibitor. The tables depict ST-Luc and TNKS2 IC_{50}-values along with cLogP-values and HLM half-lives (t½). nt = not tested. (b) A scheme of selected compound structures with graphically depicted calculated sites of metabolism (SOM). The color circles reflect the ranking of metabolic attack points based on based on SOM consensus scores (SCS). Ranking: Brown (1st), blue (2nd), yellow (3rd) and green (4th). A table

containing the SCS scores is shown in Supplementary Figure 4a. (c) Graphs showing **66** plasma concentration when dosed i.v (1mg/Kg), p.o (5mg/Kg), and i.p (5 mg/Kg) to male (black) and female (grey) ICR mice. The error bars indicate standard deviations. The compound half-lives (t½) are depicted. (d) A table summarizing the pharmacokinetic profile of **66** in ICR mice. Half life (t½), maximal concentration (C_{max}), time to reach C_{max} (T_{max}), area under the curve (AUC)($AUC_{(0-\infty)}$), AUC to last time point (24h)($AUC_{(0-t)}$), volume of distribution in the terminal phase (Vz), clearance (the volume of plasma cleared of the compound per unit time, CL), mean residence time ($MRT_{(0-\infty)}$), bioavailability (F*) and (F**) parameters are shown. F* was calculated as F (%) = ($Dose_{iv} \times AUC_{po/ip(0-t)}$) / ($Dose_{po/ip} \times AUC_{iv(0-t)}$) × 100%. F**was calculated as F (%) = ($Dose_{iv} \times AUC_{po/ip(0-\infty)}$) / ($Dose_{po/ip} \times AUC_{iv(0-\infty)}$) × 100%.

Figure 3. Drug binding pocket of 66 in the PARP domain of tankyrase 2. (a) Top view of **66** represented as sticks and colored cyan in the binding pocket of TNKS2 (pale blue). Superimposed with TNKS1 (yellow) bound with **5** (yellow). The anomalous difference Fourier map is contoured at 3.5 σ (red mesh), the peak density indicates the presence of the chloride in the region D of **66**, and thus confirm that it is stabilized in the G-loop binding pocket, formed by residues Tyr1071 to Ile1075, and assisted by His1031 to Phe1035. Residues highlighted with labels are all numbered according to TNKS2. The red arrows indicate significant molecular differences of the binding pocket between **5** and **66** upon binding. (b) TNKS1 in the apo-form (pink) is superimposed with TNKS2 and **66**. In the apo-form Tyr1203 (orange, Tankyrase 1 numbering) from the D-loop is stabilized in the pocket of the G-loop, and is likely to contribute to the specificity of **66**. Tyr1071 is maintained in a conformation equivalent to the apo-form. Therefore we assume that this represent a stabilized state, thus **66** does not need to force

molecular changes of this pocket for binding. Hydrogen bonds are shown as black dashed lines. (c) Alignment of human PARP domains 1-16. Sequence identity above 50% has been colored. Conserved hydrophobic regions in light blue (V,I,L,A), Aromatic in light cyan (H, Y, F), positive charged in blue (K, R), glycine (light brown), and serine (green). Numbering has been done according to TNKS2, (belonging to PARP5), with TNKS 1 and TNKS2 placed on top for clarity. Key residues believed to be involved in π–π interactions have been highlighted with black boxes in the alignment. Only residues highlighted in the figure (a,b) are marked with a label.

Fig.1

a

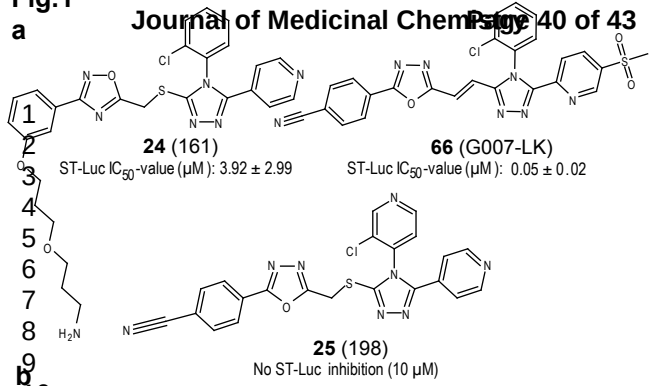

b

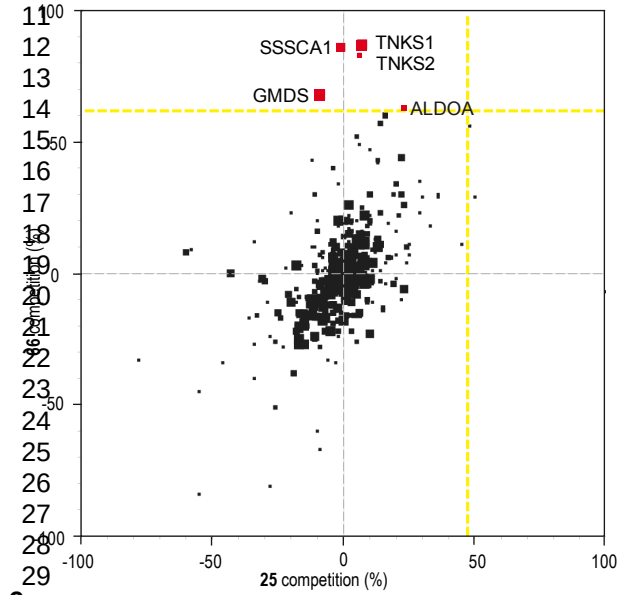

c

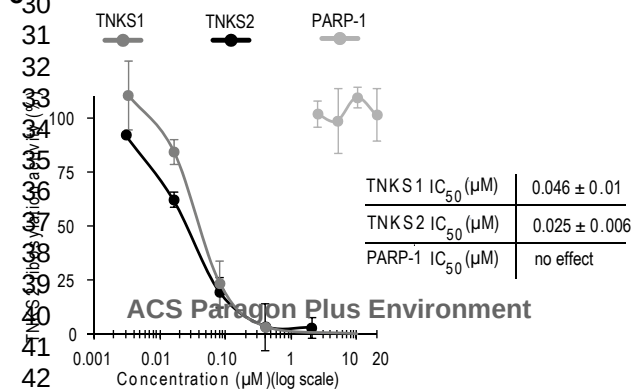

TNKS1 IC_{50} (µM)	0.046 ± 0.01
TNKS2 IC_{50} (µM)	0.025 ± 0.006
PARP-1 IC_{50} (µM)	no effect

a

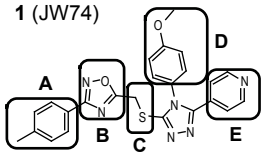

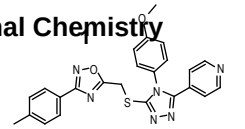

ST-Luc IC_{50}-value (μM)	1.01 ± 0.8
TNKS2 IC_{50}-value (μM)	0.46 ± 0.18
cLogP	4.7 ± 0.7
HLM t½ (min)	3

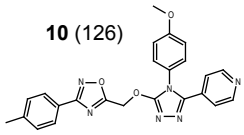

ST-Luc IC_{50}-value (μM)	>10
TNKS2 IC_{50}-value (μM)	>10
cLogP	4.3 ± 0.9
HLM t½ (min)	nt

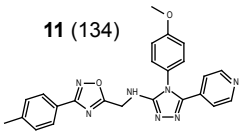

ST-Luc IC_{50}-value (μM)	>10
TNKS2 IC_{50}-value (μM)	>10
cLogP	4.1 ± 0.9
HLM t½ (min)	6.5

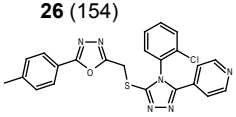

ST-Luc IC_{50}-value (μM)	0.14 ± 0.46
TNKS2 IC_{50}-value (μM)	0.051 ± 0.001
cLogP	5.1 ± 1.1
HLM t½ (min)	2.4

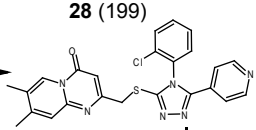

ST-Luc IC_{50}-value (μM)	4.53 ± 1.92
TNKS2 IC_{50}-value (μM)	1.8 ± 0.46
cLogP	4.0 ± 0.8
HLM t½ (min)	7

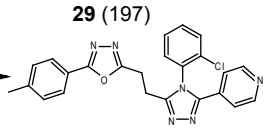

ST-Luc IC_{50}-value (μM)	0.42 ± 0.1
TNKS2 IC_{50}-value (μM)	0.29 ± 0.03
cLogP	4.9 ± 1.2
HLM t½ (min)	7

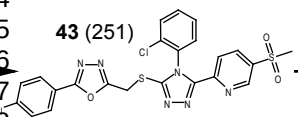

ST-Luc IC_{50}-value (μM)	0.05 ± 0.02
TNKS2 IC_{50}-value (μM)	0.043 ± 0.003
cLogP	4.9 ± 1.2
HLM t½ (min)	4

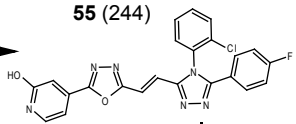

ST-Luc IC_{50}-value (μM)	6.3 ± 0.1
TNKS2 IC_{50}-value (μM)	12.3 ± 5.5
cLogP	4.8 ± 1.3
HLM t½ (min)	128

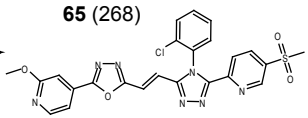

ST-Luc IC_{50}-value (μM)	0.07 ± 0.02
TNKS2 IC_{50}-value (μM)	0.054 ± 0.01
cLogP	3.5 ± 1.4
HLM t½ (min)	37

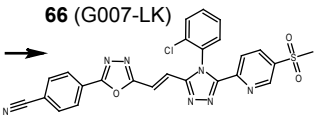

ST-Luc IC_{50}-value (μM)	0.05 ± 0.02
TNKS2 IC_{50}-value (μM)	0.025 ± 0.006
cLogP	3.9 ± 1.3
HLM t½ (min)	101

b

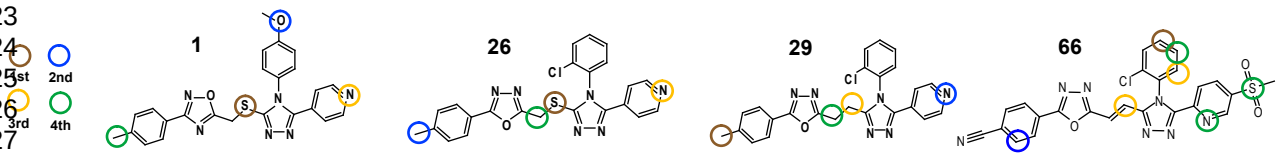

c

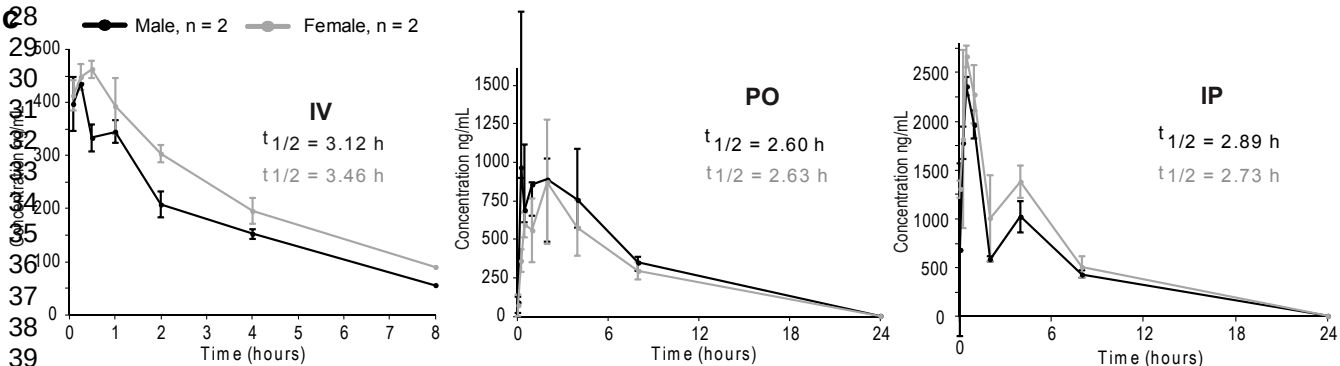

d

	Sex	$t_{1/2}$ (h)	T_{max} (h)	C_{max} (ng/mL)	$AUC_{(0-t)}$ (ng/mL*h)	$AUC_{(0-\infty)}$ (ng/mL*h)	Vz (L/kg)	CL (L/hr/kg)	$MRT_{(0-\infty)}$ (h)	F* (%)	F** (%)
IV (1 mg/kg)	Male	3.12	0.25	434	1423	1677	2.7	0.60	4.1	-	-
	Female	3.46	0.5	462	1854	2305	2.2	0.43	4.8	-	-
PO (5 mg/kg)	Male	2.60	0.25	967	8254	8269	-	-	5.1	116	99
	Female	2.63	2.0	871	6739	6750	-	-	5.1	73	59
IP (5 mg/kg)	Male	2.89	0.5	2358	11157	11193	-	-	4.8	157	133
	Female	2.73	0.5	2665	14061	14095	-	-	4.6	152	122

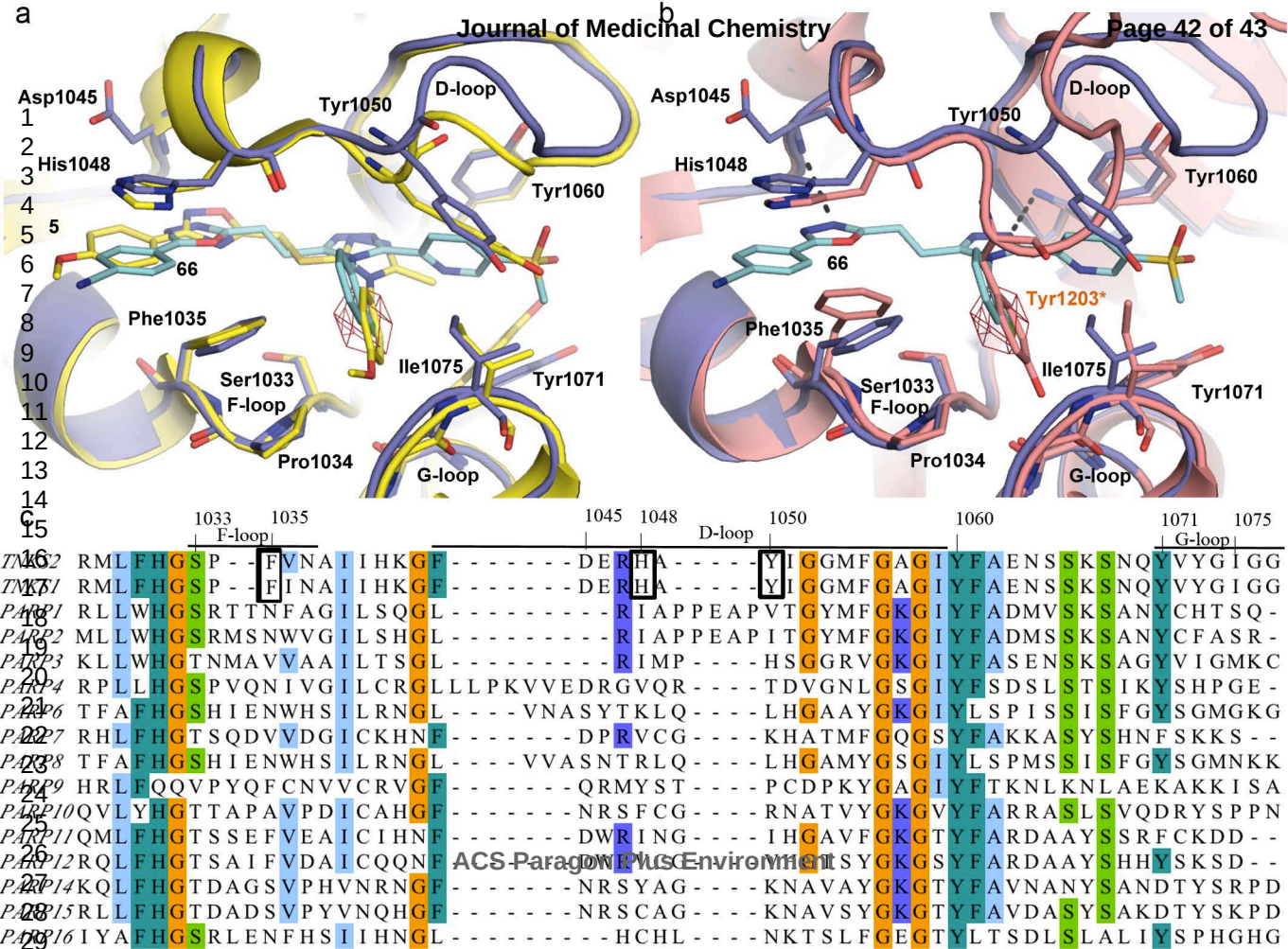

Table of Contents graphic

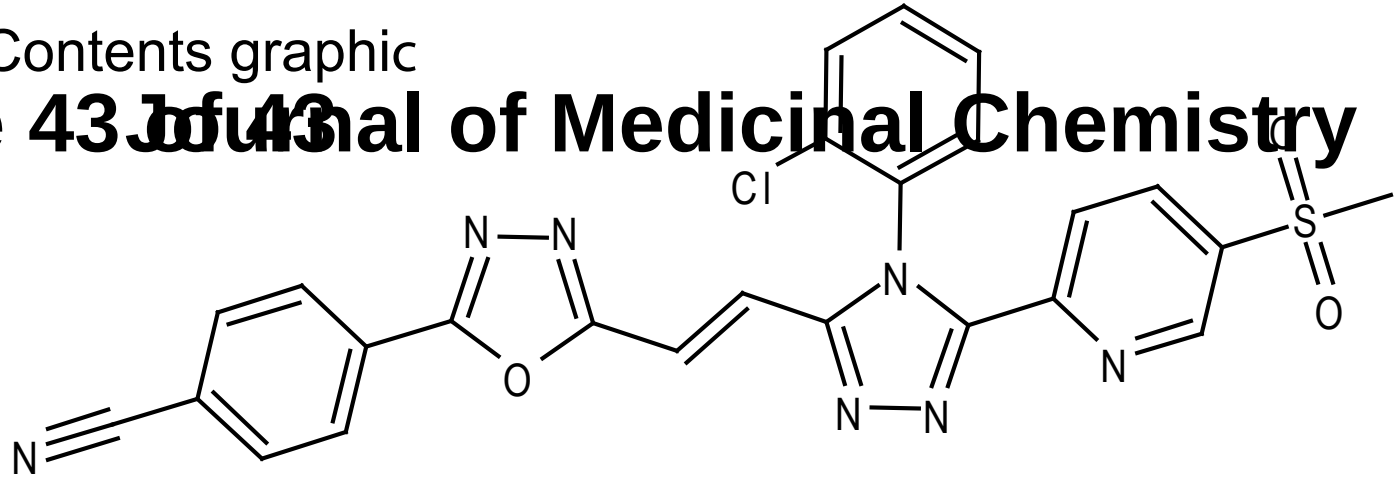

ST-Luc IC_{50}-value (μM)	0.05 ± 0.02
TNKS1 IC_{50}-value (μM)	0.046 ± 0.001
TNKS2 IC_{50}-value (μM)	0.025 ± 0.006
cLogP	3.9 ± 1.3
HLM t½ (min)	101

	Bioavailability (F)	$t_{1/2}$ (h)
IV	-	3.29
PO	94.3%	2.61
IP	>100%	2.81